JACS
JOURNAL OF THE AMERICAN CHEMICAL SOCIETY

Communication

pubs.acs.org/JACS

Formation of Hexagonal-Close Packed (HCP) Rhodium as a Size Effect

Jing Lu Huang,[†] Zhi Li,[‡] Hao Hong Duan,[‡] Zhi Ying Cheng,[†] Ya Dong Li, Jing Zhu,[†] and Rong Yu*[,†]

[†]National Center for Electron Microscopy in Beijing, School of Materials Science and Engineering, Key Laboratory of Advanced Materials of Ministry of Education of China, State Key Laboratory of New Ceramics and Fine Processing, Tsinghua University, Beijing 100084, China

[‡]Department of Chemistry, Tsinghua University, Beijing 100084, China

Supporting Information

ABSTRACT: Previous studies on the structural and functional properties of rhodium are based on the face-centered-cubic (fcc) structure in the bulk form. Here we report the first discovery of the hexagonal-close packed (hcp) rhodium in the nanoparticle form. The hcp Rh can be directly synthesized by solvothermal reaction or by electron-beam induced decomposition of Rh monolayers. The hcp Rh nanoparticles are stable under electron beam irradiation. Compared with the fcc structure, the hcp Rh nanoparticles show a large lattice expansion (6% larger atomic volume). The first-principles calculations suggest that the lower surface energy of hcp Rh leads to the size effect in the crystal structure.

The crystal structure of a material is a fundamental property that strongly affects the mechanical, electrical, magnetic, optical, and catalytic properties. In the noble metal elements (Ru, Rh, Pd, Ag, Os, Ir, Pt, Au), only Ru and Os have the hexagonal close-packed (hcp) structure in the bulk form, while all of the others, including rhodium, have the high-symmetry face-centered-cubic (fcc) structure at all temperatures.[1] The crystal structures of noble metals are stable even at high pressures, although the pressure-induced polymorphic transitions in many materials have been known for a long time.[2] Interestingly, recent studies have shown that the nanoparticles, nanowires, or nanosheets of noble metals may have different crystal structures, showing a strong size effect.[3] Ruthenium nanoparticles with fcc and hcp structures were reported to show different size dependences of the activity in CO oxidation reactions, because of the differences in the electronic states and surfaces in the fcc and hcp structures.[3a,4] Theoretical data and experimental evidence revealed that (11$\bar{2}$0) oriented hcp and dhcp palladium films deposited on W (100) show obvious ferromagnetism, in comparison to the naturally nonmagnetic fcc structured palladium bulk form.[5]

Rhodium has been extensively investigated as an effective catalyst in the reduction of nitric oxide in automobile exhaust,[6] hydrogenation reactions,[7] and asymmetric hydroformylation of olefins,[8] to name a few. In the past, studies on chemical and physical properties of rhodium were exclusively based on the fcc structure, such as the synthesis and characterization of rhodium-based catalysts,[9] the chemisorption and reaction of small-molecule gases on rhodium surfaces,[10] and the geometry, magnetic, and electronic properties of Rh clusters.[11] Very little research except a few theoretical simulations considered the hcp structure.[12] Here, we report the first experimental identification of hcp-structured rhodium, which has been obtained through two different routes.

The first route is the electron-beam induced decomposition of rhodium monolayers. During the high-resolution transmission electron microscopy experiments, we found the structure of free-standing monolayers of Rh to be sensitive to high energy electron irradiation. Because of the large surface energy of Rh monolayers, some atoms would pile up to form nanocrystals, leaving nanovoids in the remaining monolayers. A typical aberration-corrected TEM image of the nanoparticles and the corresponding diffractogram are given in Figure 1a and

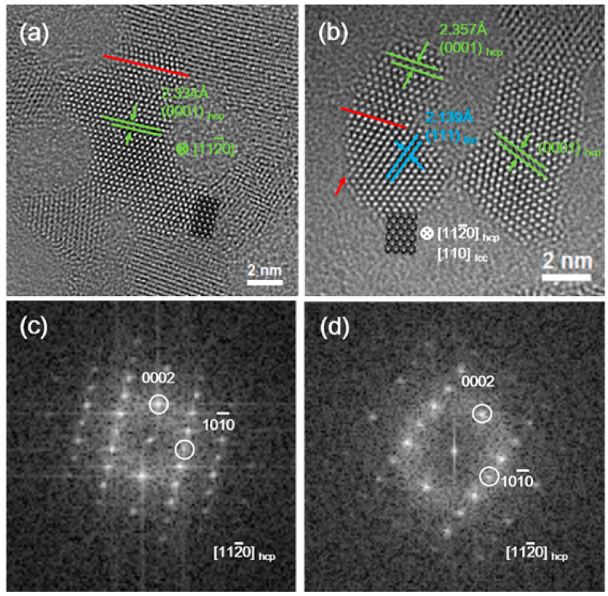

Figure 1. Typical aberration-corrected TEM images of rhodium nanoparticles prepared via (a) the electron-beam induced decomposition of Rh monolayers, and (b) the solvent thermal synthesis. The electron diffractograms are shown in (c) and (d), respectively. As indexed in the diffractograms, the particles have the hcp structure, except the bottom left part in (b), which has the fcc structure.

Received: September 26, 2016
Published: January 3, 2017

DOI: 10.1021/jacs.6b09730
J. Am. Chem. Soc. 2017, 139, 575−578

1b, respectively, showing the hcp structure viewed along the [11$\bar{2}$0] zone axis. The inset shows a simulated image of the hcp structure, which matches well with with the experimental image. At the top edge of the particle, there is a thin layer of the fcc structure viewed along the [110] zone axis, as outlined by a red line.

Figure 1b shows a typical image of the nanoparticles synthesized directly using the solvent thermal method. There were two nanoparticles: the right one is an hcp particle observed along the [11$\bar{2}$0] direction, while the left one consisted of an hcp particle (upper part) and an fcc particle (bottom part). The inset shows a simulated image of the fcc structure. The red arrow indicates a twin boundary in the fcc particle.

For all the hcp particles identified, the lattice parameters were measured to be a_{hcp} = 2.78 Å and c_{hcp} = 4.64 Å, giving the unit cell volume of 31.1 Å^3, or 15.5 Å^3 per atom. The lattice parameter of the fcc particles was measured to be a_{fcc} = 3.88 Å, giving the unit cell volume of 58.4 Å^3, or 14.6 Å^3 per atom.

Figure 2 shows the equations of state for bulk fcc and hcp structures calculated with the first-principles method. The

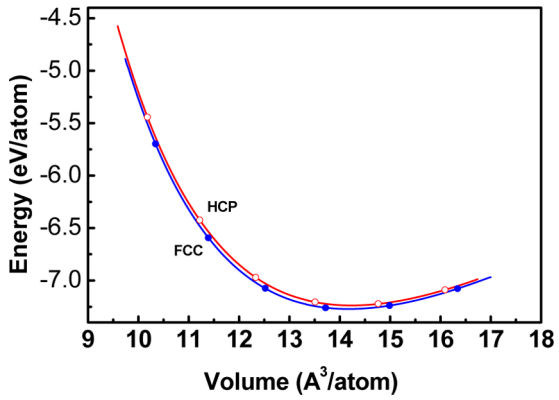

Figure 2. Equations of state of the fcc and hcp structures of Rh. In the bulk form, the hcp structure has negligible lattice expansion relative to the fcc structure.

energy of the hcp structure is higher than that of the fcc structure up to 200 GPa. It is consistent with the fact that the bulk form of the hcp structure has never been observed before. The optimized lattice parameters of the hcp structure are a_{hcp} = 2.722 Å and c_{hcp} = 4.386 Å, giving the unit cell volume of 28.46 Å^3, or 14.23 Å^3 per atom. The optimized lattice parameters of the fcc structure are a_{fcc} = 3.829 Å, giving the unit cell volume of 56.70 Å^3, or 14.17 Å^3 per atom. For the DFT calculations with the GGA approximation (used in this study), it is usual that the absolute lattice parameters are slightly overestimated, and the bulk modulus is underestimated, but the relative values can be well reproduced. In the bulk form, the hcp structure has a small volume expansion (0.4%) relative to the fcc structure. The bulk moduli of the two structures also have the same value (252 GPa).

Lattice strain is considered to play an important role in the catalytic reactions.[13] Previously, a large amount of studies revealed that the lattice strain in the surfaces of Rh changes the adsorption of atoms or molecules on the surfaces.[14] Mavrikakis et al. found that surface reactivity increases with lattice expansion, following a concurrent upshift of the metal d states.[15]

Although the hcp structure has a small volume expansion (0.4%) relative to the fcc structure in the bulk form, the measured hcp nanoparticles have a volume expansion of 6% relative to the fcc nanoparticles. According to the equations of state, a volume change of 6% would require a pressure as high as 20 GPa in the bulk form. This "huge" lattice expansion of the hcp nanoparticles can be well noticed in the following two-dimensional lattice mapping of the two structures. We measured the strain distributions in the Rh nanoparticles of both hcp and fcc structures. Here we use the area of the triangles formed by the nearest neighbors to represent the lattice expansion, which is shown in Figure 3a and 3b. It is

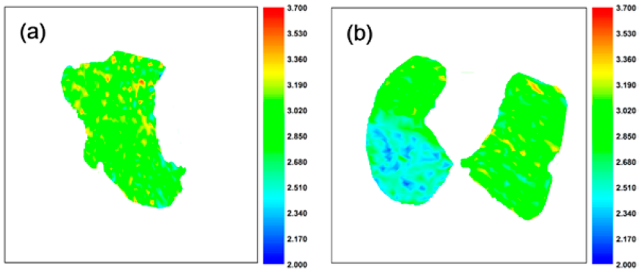

Figure 3. Strain mapping in the nanoparticles shown in Figure 1. There is large lattice expansion in the hcp nanoparticles.

obvious that the lattice of the hcp structure is significantly expanded relative to the fcc structure, consistent with the measured lattice parameters described above. The large lattice expansion in the hcp structure provides another factor to tune the reactivity and/or selectivity of Rh-based catalysts.

At the nanometer scale, the surface properties are of crucial importance for the structural stability and practical applications. Surface energy and work function are the two fundamental properties of metal catalysts that influence a wide range of surface phenomena in the preparation and application of catalysts, including the grain shape, the formation of grain boundaries, and the adsorption and desorption in catalytic reactions.[11b,16] In this study, the surface energies and work functions of surfaces of hcp and fcc Rh have been investigated using first-principles calculations.

Several low-index surfaces, i.e. $(111)_{fcc}$, $(110)_{fcc}$, $(100)_{fcc}$, $(311)_{fcc}$, $(11\bar{2}0)_{hcp}$, $(0001)_{hcp}$, $(10\bar{1}0)_{hcp}$, and $(10\bar{1}2)_{hcp}$, have been studied. For each surface, a series of models with a thickness range of 2−20 Å were considered. The calculated surface energies are plotted in Figure 4. For the hcp rhodium,

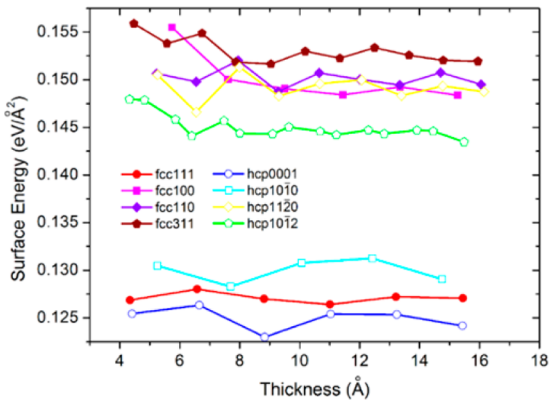

Figure 4. Surface energies of low index surfaces in fcc and hcp Rh.

DOI: 10.1021/jacs.6b09730
J. Am. Chem. Soc. 2017, 139, 575−578

there are two low energy surfaces, (0001) and $(10\bar{1}0)$, while the fcc rhodium has only one, (111). Their surface energies have the order $(0001)_{hcp} < (111)_{fcc} < (10\bar{1}0)_{hcp}$. Furthermore, high energy surfaces of hcp Rh are generally more stable than those of fcc Rh, with the order $(10\bar{1}2)_{hcp} < (11\bar{2}0)_{hcp} \approx (100)_{fcc} \approx (110)_{fcc} < (311)_{fcc}$. Therefore, from the surface energy point of view, the small size would stabilize the hcp Rh, which has a lower energy surface relative to the fcc structure.

Additionally, surface energies show different degrees of size dependence. The low energy surfaces, such as $(0001)_{hcp}$, $(111)_{fcc}$, and $(10\bar{1}0)_{hcp}$, show little size dependence. For the surfaces with relatively higher energies, however, the surface energies increase rapidly with as the thickness decreases to less than 10 Å. In our experiments, the size of the Rh particles are in the range 1−5 nm; thus, further theoretical analyses are based on the data from the surface models with a thickness of ∼15 Å.

The work functions of the low-index surfaces were also calculated, as shown in Figure 5. They are in the range 4.3−5.3 eV, in the order $(0001)_{hcp} > (111)_{fcc} > (10\bar{1}0)_{hcp} \approx (100)_{fcc} > (10\bar{1}2)_{hcp} \approx (311)_{fcc} > (11\bar{2}0)_{hcp} \approx (110)_{fcc}$. The trend follows the empirical rule that the work function is lower for loosely packed surfaces, which have relatively higher energies.[17]

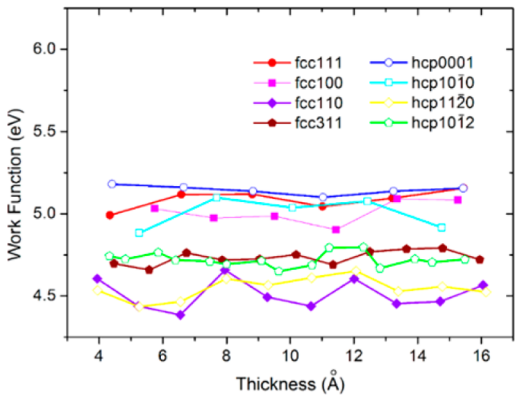

Figure 5. Work functions of Rh in the hcp and fcc structures.

An understanding of the relative stability and formation mechanism of the hcp Rh is necessary for efficient synthesis and further study of its properties. Based on the first-principles calculations and Wulff construction method, the surface energy and total energy of nanoparticles of fcc and hcp Rh were calculated. The Wulff construction is a method to determine the equilibrium shape of a crystal, as shown in Figure 6. The Gibbs−Wulff theorem says that the length of a vector drawn from the crystal center and normal to a crystal face will be proportional to its surface energy. Table 1 lists the main simulation results. For fcc Rh, there are 8 (111) facets, 6 (100) facets, 12 (110) facets, and 24 (311) facets. Among them, the (111) facet as the lowest energy surface occupies 66.95% of the total surface area. For hcp Rh, there were 2 (0001) facets, 6 $(10\bar{1}0)$ facets, and 12 $(10\bar{1}2)$ facets. There are no $(11\bar{2}0)$ facets due to its high energy. The two low energy surfaces (0001) and $(10\bar{1}0)$ occupy 62.26% of the total surface area. For particles of equal volume, the surface energy of hcp Rh is lower than that of fcc Rh.

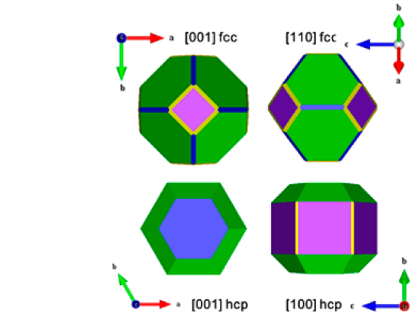

Figure 6. Equilibrium crystal shapes of fcc Rh and hcp Rh simulated by Wulff construction method.

Table 1. Main Parameters of Equilibrium Crystal Shapes Simulated by Wulff Construction Method[a]

structure	surface	surface energy [eV/Å^2]	number of facets	area proportion
FCC	111	0.1271	8	66.95%
	100	0.1484	6	14.83%
	110	0.1507	12	6.36%
	311	0.1520	24	11.86%
HCP	0001	0.1242	2	16.92%
	$10\bar{1}0$	0.1290	6	45.34%
	$10\bar{1}2$	0.1435	12	37.74%
	$11\bar{2}0$	0.1493	–	0.00%

[a]Surface energies for slabs of about 15 Å thick were used.

Figure 7 shows the total energies of fcc Rh and hcp Rh as a function of particle volume. Since the bulk energy of fcc Rh (−7.26 eV/atom) is lower than that of hcp Rh (−7.23 eV/atom), the total energy of the hcp particle is still higher than that of the fcc particle in the size range considered in this work, consistent with the fact that there are still more particles in fcc than in the hcp structure. As the particle size decreases, however, the proportion of the surfaces increases. As a result, the lower surface energy of the hcp structure would compensate the bulk energy to a larger extent at smaller particle sizes, giving a smaller energy difference between the two structures.

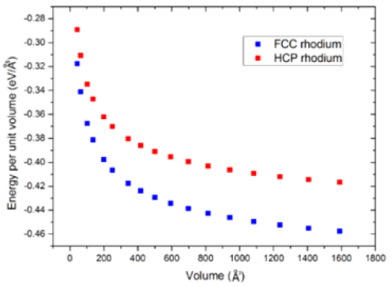

Figure 7. Size-dependence of the total energies of fcc Rh and hcp Rh. The energy difference between the two structures becomes smaller as the volume decreases.

As the particle size becomes too small, say less than 100 atoms (about 1.3 nm in diameter), most atoms being present at the surfaces, the division of the total energy into the bulk and surface energies would be less reliable. In this case, all the atoms in the particle have to be treated on an equal footing. Therefore, the relative stability of the hcp and fcc nanoparticles becomes a structure problem of clusters. We note that Chien et al. predicted low energy Rh clusters with the hcp stacking sequence.[12] It is highly possible that the hcp stacking forms at

DOI: 10.1021/jacs.6b09730
J. Am. Chem. Soc. 2017, 139, 575−578

the nucleation stage, where the particle size is so small that the hcp stacking is more stable than the fcc stacking.

As described above, the hcp-type Rh nanoparticles can be formed by either electron-irradiation-induced decomposition of Rh monolayers or directly synthesized by solvothermal reaction, and the hcp-type would not transform into the fcc structure during the observation in TEM. It indicates that the hcp-type Rh is intrinsically stable at a very small size. This is in contrast to the case of gold. Huang et al.[3b] found that the irradiation of a high-energy electron may induce the transformation of gold from the metastable hcp structure to the fcc structure, which is the stable structure for gold in both the bulk and nanoparticle forms. Compared with gold, the high stability of the hcp Rh nanoparticles can be attributed to its high melting point [T_m(Au) = 1064 °C, and T_m(Rh) = 1964 °C]. Therefore, it would require much higher energies to induce phase transformations in Rh.

In summary, quantitative analysis using aberration-corrected high-resolution transmission electron microscopy reveals the existence of hcp Rh and a large lattice expansion in the new phase compared with the well-known fcc Rh. Theoretical calculations indicated that the lower surface energy of Rh provides the stability for hcp Rh at small sizes. Although the bulk energy of hcp Rh is higher than that of fcc Rh, as the size of the nanoparticles decreases, the surface energy plays a more important role, leading to stable hcp Rh. Systematic experimental and theoretical studies are required to answer questions such as, "At what exact size the hcp structure is more stable than fcc?", "How the temperature affect the relative stability?", "Can alloying with other elements or the adsorption of molecules modify the structure?, and How?". The answers to these questions would guide the synthesis of pure hcp Rh nanoparticles and give a clearer picture about the physical and chemical properties of Rh.

■ ASSOCIATED CONTENT

Supporting Information

The Supporting Information is available free of charge on the ACS Publications website at DOI: 10.1021/jacs.6b09730.

Experimental details, synthesis, structural characterization, preferred growth direction, XRD, and density-functional theory calculations (PDF)

■ AUTHOR INFORMATION

Corresponding Author

*ryu@tsinghua.edu.cn

ORCID

Rong Yu: 0000-0003-1687-3597

Notes

The authors declare no competing financial interest.

■ ACKNOWLEDGMENTS

This work was supported by NSFC (51525102, 51371102, 51390475) and National Basic Research Program of China (2015CB654902). In this work we used the resources of the National Center for Electron Microscopy in Beijing, Shanghai Supercomputer Center, and Tsinghua National Laboratory for Information Science and Technology.

■ REFERENCES

(1) Pearson, W. B. *A Handbook of Lattice Spacings and Structures of Metals and Alloys*, Vol. 2; Pergamon Press: Oxford, 1967.

(2) Bridgman, P. W. *The Physics of High Pressure*; G. Bell and Sons: London, 1952.

(3) (a) Kusada, K.; Kobayashi, H.; Yamamoto, T.; Matsumura, S.; Sumi, N.; Sato, K.; Nagaoka, K.; Kubota, Y.; Kitagawa, H. *J. Am. Chem. Soc.* **2013**, *135*, 5493. (b) Huang, X.; Li, S.; Huang, Y.; Wu, S.; Zhou, X.; Li, S.; Gan, C. L.; Boey, F.; Mirkin, C. A.; Zhang, H. *Nat. Commun.* **2011**, *2*, 292. (c) Ye, H.; Wang, Q.; Catalano, M.; Lu, N.; Vermeylen, J.; Kim, M. J.; Liu, Y.; Sun, Y.; Xia, X. *Nano Lett.* **2016**, *16*, 2812. (d) Fan, Z.; Zhang, H. *Chem. Soc. Rev.* **2016**, *45*, 63. (e) Fan, Z.; Zhang, X.; Yang, J.; Wu, X.; Liu, Z.; Huang, W.; Zhang, H. *J. Am. Chem. Soc.* **2015**, *137*, 10910. (f) Fan, Z.; Luo, Z.; Huang, X.; Li, B.; Chen, Y.; Wang, J.; Hu, Y.; Zhang, H. *J. Am. Chem. Soc.* **2016**, *138*, 1414. (g) Fan, Z.; Huang, X.; Han, Y.; Bosman, M.; Wang, Q.; Zhu, Y.; Liu, Q.; Li, B.; Zeng, Z.; Wu, J.; Shi, W.; Li, S.; Gan, C.; Huang, Z. *Nat. Commun.* **2015**, *6*, 6571.

(4) (a) Joo, S. H.; Park, J. Y.; Renzas, J. R.; Butcher, D. R.; Huang, W.; Somorjai, G. A. *Nano Lett.* **2010**, *10*, 2709. (b) Song, C.; Sakata, O.; Kumara, L. S. R.; Kohara, S.; Yang, A.; Kusada, K.; Kobayashi, H.; Kitagawa, H. *Sci. Rep.* **2016**, *6*, 31400. (c) Kusada, K.; Kitagawa, H. *Adv. Mater.* **2016**, *28*, 1129.

(5) Huger, E.; Osuch, K. *Europhys. Lett.* **2003**, *63*, 90.

(6) (a) Belton, D. N.; Dimaggio, C. L.; Schmieg, S. J.; Ng, K. Y. S. *J. Catal.* **1995**, *157*, 559. (b) Hirano, H.; Yamada, T.; Tanaka, K. I.; Siera, J.; Cobden, P.; Nieuwenhuys, B. E. *Surf. Sci.* **1992**, *262*, 97.

(7) Harada, T.; Ikeda, S.; Ng, Y. H.; Sakata, T.; Mori, H.; Torimoto, T.; Matsumura, M. *Adv. Funct. Mater.* **2008**, *18*, 2190.

(8) (a) Gross, E.; Liu, J. H.; Alayoglu, S.; Marcus, M. A.; Fakra, S. C.; Toste, F. D.; Somorjai, G. A. *J. Am. Chem. Soc.* **2013**, *135*, 3881. (b) Wang, X.; Buchwald, S. L. *J. Am. Chem. Soc.* **2011**, *133*, 19080.

(9) (a) Kroner, A. B.; Newton, M. A.; Tromp, M.; Russell, A. E.; Dent, A. J.; Evans, J. *ChemPhysChem* **2013**, *14*, 3606. (b) Grass, M. E.; Joo, S. H.; Zhang, Y.; Somorjai, G. A. *J. Phys. Chem. C* **2009**, *113*, 8616. (c) Yuan, Y.; Yan, N.; Dyson, P. J. *ACS Catal.* **2012**, *2*, 1057. (d) Alayoglu, S.; Eichhorn, B. *J. Am. Chem. Soc.* **2008**, *130*, 17479.

(10) (a) Castner, D. G.; Sexton, B. A.; Somorjai, G. A. *Surf. Sci.* **1978**, *71*, 519. (b) Ohtani, H.; Wilson, R. J.; Chiang, S.; Mate, C. M. *Phys. Rev. Lett.* **1988**, *60*, 2398. (c) Root, T. W.; Schmidt, L. D.; Fisher, G. B. *Surf. Sci.* **1985**, *150*, 173.

(11) (a) Sun, H.; Ren, Y.; Luo, Y.-H.; Wang, G. H. *Phys. B* **2001**, *293*, 260. (b) Popa, C.; van Bavel, A. P.; van Santen, R. A.; Flipse, C. F. J.; Jansen, A. P. *Surf. Sci.* **2008**, *602*, 2189.

(12) Chien, C.-H.; Blaisten-Barojas, E. *J. Chem. Phys.* **2000**, *112*, 2301.

(13) Wu, J.; Li, P.; Pan, Y. T.; Warren, S.; Yin, X.; Yang, H. *Chem. Soc. Rev.* **2012**, *41*, 8066.

(14) (a) Gómez, R.; Javier Gutiérrez de Dios, F.; Feliu, J. M. *Electrochim. Acta* **2004**, *49*, 1195. (b) Flege, J. I.; Sutter, P. *Phys. Rev. B: Condens. Matter Mater. Phys.* **2008**, *78*, 78. (c) Gan, L.; Yu, R.; Luo, J.; Cheng, Z. Y.; Zhu, J. *J. Phys. Chem. Lett.* **2012**, *3*, 934.

(15) Mavrikakis, M.; Hammer, B.; Nørskov, J. K. *Phys. Rev. Lett.* **1998**, *81*, 2819.

(16) Skriver, H. L.; Rosengaard, N. M. *Phys. Rev. B: Condens. Matter Mater. Phys.* **1992**, *46*, 7157.

(17) Oura, K.; Lifshits, V. G.; Saranin, A. A.; Zotov, A. V.; Katayama, M. *Surf. Sci.*; Springer-Verlag: Belin, 2003.

DOI: 10.1021/jacs.6b09730
J. Am. Chem. Soc. 2017, 139, 575−578